

Research Article

Cite this article: Wang S, Wu X, Yang Y, Zhu C, Wu Z, Xia C (2020). Hybrid modeling and control of ICPT system with synchronous three-phase triple-parallel Buck converter. *Wireless Power Transfer* 7, 10–18. <https://doi.org/10.1017/wpt.2019.17>

Received: 28 August 2019
Revised: 14 November 2019
Accepted: 14 December 2019
First published online: 28 January 2020


Key words:

Constant voltage; current sharing; ICPT; synchronous; three-phase triple-parallel

Author for correspondence:

Chenyang Xia, School of Electrical and Power Engineering, China University of Mining and Technology, Xuzhou 221116, China.
E-mail: bluesky198210@163.com

Hybrid modeling and control of ICPT system with synchronous three-phase triple-parallel Buck converter

Songcen Wang¹, Xiaokang Wu¹, Ying Yang², Cong Zhu², Zhen Wu² and Chenyang Xia² 

¹China Electric Power Research Institute, Beijing 100192, China and ²School of Electrical and Power Engineering, China University of Mining and Technology, Xuzhou 221116, China

Abstract

Aiming at the influence of coupling coefficient variation on the output voltage of a high-power LCC-S topology inductively coupled power transfer (ICPT) system, a synchronous three-phase triple-parallel Buck converter is used as the voltage adjustment unit. The control method for the three-phase current sharing of synchronous three-phase triple-parallel Buck converter and the constant voltage output ICPT system under the coupling coefficient variation is studied. Firstly, the hybrid model consisting of the circuit averaging model of the three-phase triple-parallel Buck converter and the generalized state-space average model for the LCC-S type ICPT system is established. Then, the control methods for three-phase current sharing of the synchronous three-phase triple-parallel Buck converter and constant voltage output of ICPT system are studied to achieve the multi-objective integrated control of the system. Finally, a 3.3 kW wireless charging system platform is built, the experimental results have verified the effectiveness of the proposed modeling and control method, and demonstrated the stability of the ICPT system.

Introduction

The inductively coupled power transfer (ICPT) technology [1–3] is widely researched and applied in the field of wireless charging because of its ability to realize large power transmission [4–6]. For the electric vehicle wireless charging system, due to the flatness of the site and the parking angle, the mutual inductance of the ICPT system will have a range of variation, which will affect the output voltage of the system. Therefore, the realization of constant voltage output [7, 8] with a DC-DC converter [9, 10] or a phase-shifting inverter [11] under the variation of mutual has been widely used. At present, the asynchronous signal-phase Buck converter is mostly used as the DC-DC converter. However, a single-phase Buck converter has insufficient voltage and current stress of the switching tubes, a large ripple of output voltage and current, and poor safety redundancy characteristics [12, 13], and it cannot be used in the high-power ICPT system. In addition, for an asynchronous single-phase Buck converter, the loss of the flyback diode is very large, and the efficiency of the asynchronous single-phase Buck converter is also not too high.

As the three-phase triple-parallel Buck converter can reduce the current stress of the power switch tube, the current ripple of the output voltage and the volume of the inductor and capacitor can be smaller. At the same time, because the synchronous DC-DC converter has a higher efficiency than the traditional asynchronous DC-DC converter, in order to reduce the conduction loss and improve the efficiency, a synchronous three-phase triple-parallel Buck converter is adopted to achieve the constant voltage output under the coupling coefficient variation in this paper, which can reduce the current stress of the power switch tube, the current ripple of the output voltage, and increase the power density of the ICPT system [14, 15].

In this paper, an LCC-S topology ICPT system with a synchronous three-phase triple-parallel Buck converter is studied. It can be divided into the front part of the three-phase triple-parallel Buck converter and the later part of the LCC-S topology resonant converter. However, as we know, this kind of system is a typical high-order non-linear system. For the later LCC-S topology resonant converter, due to the existence of inverter circuit, rectifier circuit, and resonance compensation network, and a large number of capacitance or inductance parameters in the system shows oscillation characteristics, the modeling method is not the same as the modeling method of the front three-phase triple-parallel Buck converter. Thus, the generalized state-space average (GSSA) model is used to model the LCC-S resonant converter, while small-signal modeling is used to model the three-phase triple-parallel Buck converter, so hybrid modeling of ICPT system with synchronous three-phase triple-parallel Buck

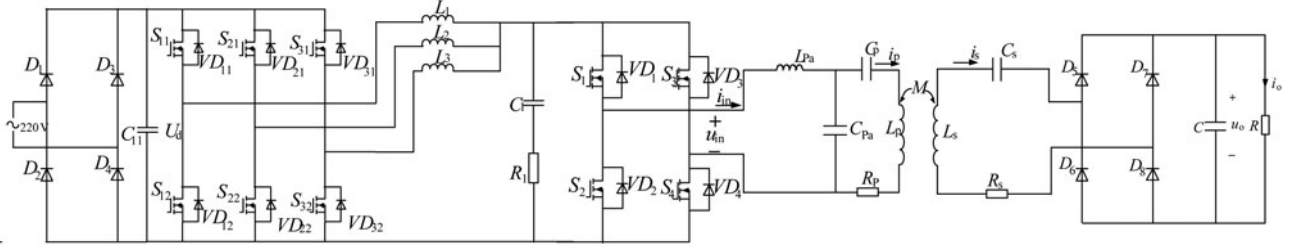


Figure 1. Schematic diagram of the ICPT system based on the synchronous three-phase triple-parallel Buck converter.

converter is studied. In addition, based on the frequency-domain method, the methods of the three-phase current sharing of the synchronous three-phase triple-parallel Buck converter and the constant voltage output control of the ICPT system under coupling coefficient variation are studied. Firstly, based on the circuit average method and GSSA method, the mathematical model of the ICPT system is established. Then, the current sharing and constant voltage output closed-loop controller under the coupling coefficient variation is designed by using the frequency-domain method. Finally, an experimental platform is built and tested to validate the effectiveness of the current sharing and constant voltage output controller.

Structure and modeling of ICPT system with a synchronous three-phase triple-parallel Buck converter

Synchronous three-phase triple-parallel Buck converter ICPT system

In this paper, the design objective of the ICPT system is that the input voltage is 220 VAC, the output voltage is 300 VDC, the wireless transmission distance is 15 cm, the output power is 3.3 kW, and the system operating frequency of the inverter is 85 kHz. In order to realize the constant voltage output of the system with the coupling coefficient variation, a three-phase triple-parallel parallel Buck converter is used in the primary circuit of the ICPT system. The structure of the ICPT system with a synchronous three-phase triple-parallel parallel Buck converter is shown in Fig. 1.

In Fig. 1, D_1 – D_4 constitutes the primary rectifier circuit. D_5 – D_8 constitutes the secondary rectifier circuit. S_{11} – S_{31} and S_{12} – S_{32} are the upper and lower power switches of the synchronous three-phase triple-parallel Buck converter. L_1 , L_2 , L_3 , and C_1 constitute the filter of the Buck converter. S_1 – S_4 constitutes the high-frequency inverter. L_{pa} , C_{pa} , C_p , and L_p constitute the LCC compensation topology on the primary side, and L_p is the equivalent inductance of the transmitting coil. L_s and C_s are the equivalent inductance and compensation capacitor of the secondary side, respectively, which constitute the series compensation topology of the secondary side. R is the equivalent load of the ICPT system.

Hybrid modeling and analysis for the synchronous three-phase triple-parallel Buck converter ICPT system

In order to design the closed-loop controller of the system, the mathematical model of the system based on the frequency-domain analysis method must be established in advance. As shown in Fig. 1, it consists of a synchronous three-phase triple-parallel Buck converter and an LCC-S topology resonant converter. As we know, this kind of system is a typical high-order

non-linear system. For the later LCC-S topology ICPT system, due to the existence of inverter circuit, rectifier circuit, and resonance compensation network, and a large number of capacitance or inductance parameters in the system shows oscillation characteristics, the modeling method is not the same as the modeling method of the front three-phase triple-parallel Buck converter. Thus, the GSSA model is used to model the LCC-S resonant converter [16], while a small-signal modeling method is used to model three-phase triple-parallel Buck converter, so a hybrid modeling of ICPT system with the synchronous three-phase triple-parallel Buck converter is studied.

Small-signal modeling and analysis for the synchronous three-phase triple-parallel Buck converter

The small-signal model of a single-phase synchronous Buck converter based on the network theory of a three-phase switching device is given in [17]. Based on this, the equivalent model of the synchronous three-phase triple-parallel Buck converter can be established, which is shown in Fig. 2.

According to Fig. 2, based on the small-signal model theory, the transfer function of output voltage v_o and inductor current i_L with respect to the duty cycle can be derived as

$$G_{vd}(s) = \frac{\widehat{v}_o(s)}{\widehat{d}(s)} = \frac{V_d(1 + sR_{esr}C)}{\frac{1}{3}LC\left(1 + \frac{R_{esr}}{R}\right)s^2 + \left(\frac{L}{3R} + R_{esr}C\right)s + 1}, \quad (1)$$

$$G_{id}(s) = \frac{\widehat{i}_L(s)}{\widehat{d}(s)} = \frac{V_d\left[\left(1 + \frac{R_{esr}}{R}\right)Cs + \frac{1}{R}\right]}{\frac{1}{3}LC\left(1 + \frac{R_{esr}}{R}\right)s^2 + \left(\frac{L}{3R} + R_{esr}C\right)s + 1}. \quad (2)$$

GSSA modeling and analysis for LCC-S topology resonant converter

As discussed in [16], the GSSA model is used to describe the time-domain periodic signal in the Fourier complex exponential form. By approximating the original signal with conjugate low-order harmonic components and linearly processing the non-linear link according to the properties of the Fourier coefficients, the envelope of the original signal and its approximate solution can be obtained.

According to the topology diagram of the LCC-S type resonant converter shown in Fig. 1, the Norton equivalent circuit can be obtained as in Fig. 3.

Choosing the inductor current i_{Lpa} , i_p , i_s and the capacitor voltage u_{Cpa} , u_{Cp} , u_{Cs} , u_c as the state variables. Using the linear, differential, and convolution properties of the Fourier series, the

differential equations of the system can be approximately linearized as equation (3).

$$\begin{cases} \frac{d\langle i_{L_{pa}} \rangle_1}{dt} = -\frac{1}{L_{pa}} \langle u_{C_p} \rangle_1 - \frac{2j}{L_{p2}} U_{in} - j\omega_0 \langle i_{L_{pa}} \rangle_1 \\ \frac{d\langle u_{C_{pa}} \rangle_1}{dt} = \frac{1}{C_{pa}} \langle i_{L_{pa}} \rangle_1 + \frac{1}{C_{pa}} \langle i_p \rangle_1 - j\omega_0 \langle u_{C_{pa}} \rangle_1 \\ \frac{d\langle u_{C_p} \rangle_1}{dt} = \frac{1}{C_p} \langle i_p \rangle_1 - j\omega_0 \langle u_{C_p} \rangle_1 - j\omega_0 \langle u_{C_{pa}} \rangle_1 \\ \frac{d\langle i_p \rangle_1}{dt} = \frac{L_s}{\det} \langle u_{C_{pa}} \rangle_1 - \frac{L_s}{\det} \langle u_{C_p} \rangle_1 - \frac{L_s R_p}{\det} \langle i_p \rangle_1 + \frac{M R_s}{\det} \langle i_s \rangle_1 - \frac{M}{\det} \langle u_{C_s} \rangle_1 + \frac{2Mj}{\det \pi} \langle U_o \rangle_0 - j\omega_0 \langle i_p \rangle_1 \\ \frac{d\langle i_s \rangle_1}{dt} = \frac{M}{\det} \langle u_{C_{pa}} \rangle_1 - \frac{M}{\det} \langle u_{C_p} \rangle_1 - \frac{M R_p}{\det} \langle i_p \rangle_1 + \frac{L_p R_s}{\det} \langle i_s \rangle_1 - \frac{L_p}{\det} \langle u_{C_s} \rangle_1 + \frac{2Mj}{\det \pi} \langle U_o \rangle_0 - j\omega_0 \langle i_s \rangle_1 \\ \frac{d\langle u_{C_s} \rangle_1}{dt} = \frac{1}{C_s} \langle i_s \rangle_1 - j\omega_0 \langle u_{C_s} \rangle_1 \\ \frac{d\langle U_o \rangle_0}{dt} = -\frac{2j}{C\pi} \langle i_s \rangle_{-1} + \frac{2j}{C\pi} \langle i_s \rangle_1 - \frac{1}{CR} \langle U_o \rangle_0. \end{cases} \quad (3)$$

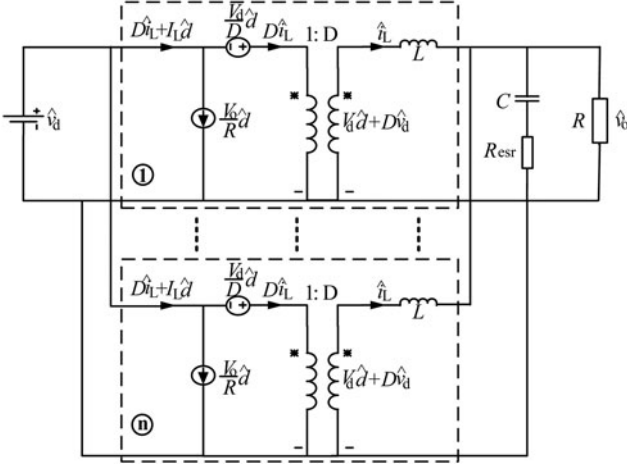


Figure 2. Small-signal model of a synchronous three-phase triple-parallel parallel Buck converter.

Then the generalized state-space equation of the LCC-S topological resonant converter can be described as

$$\begin{cases} \dot{x}(t) = Ax(t) + Bu(t) \\ y(t) = Cx(t) + Du(t) \end{cases} \quad (4)$$

where, $u(t) = [U_{in}]$ is the input voltage, $y(t) = [U_{out}]$ is the voltage of the load, and A , B , C , and D are the coefficient matrix in the GSSA equation, respectively ($A \in \mathbb{C}^{13 \times 13}$, $B \in \mathbb{C}^{13 \times 1}$, $C \in \mathbb{C}^{1 \times 13}$, $D \in \mathbb{C}^{1 \times 1}$). Then the small-signal transfer function of the LCC-S resonant converter can be obtained as

$$G_v(s) = C(sI - A)^{-1}B + D. \quad (5)$$

Design of ICPT system current sharing constant voltage output closed-loop system

In this paper, the front three-phase triple-parallel Buck converter is adopted to realize the constant voltage output under the coupling coefficient variation. The current in the three inductors may be unequal, which will make the switch of one of the phases to afford larger voltage and current stresses so as to destroy them [18]. Therefore, the current sharing control should be taken in the design.

In order to realize the current and voltage output with a closed-loop controller is proposed in this paper, which is shown in Fig. 4.

In order to facilitate the design of the voltage compensation network and current compensation networks, the current sharing and constant voltage output control of the ICPT system can be transformed into a system control block diagram, which is shown in Fig. 5.

In Fig. 5, $H_i(s)$ and $H_v(s)$ are the current and voltage feedback transfer functions, $G_{cv}(s)$ and $G_{uc_i}(s)$ are the voltage external loop compensation network and current inner loop compensation network transfer function, respectively, $G_m(s)$ is the pulse width modulation transfer function. $Z(s)$ is the output impedance, $G_{id}(s)$ is the transfer function of the converter output current with respect to the duty cycle of the control variable, and $G_r(s)$ is the transfer function of the ICPT resonant converter. The next step is to design the current loop compensation network.

Current sharing controller design

In order to analyze the system characteristics, the parameters of the system are listed in Table 1.

Set the current and voltage feedback transfer function and the carrier amplitude as 1, and the open-loop gain of the

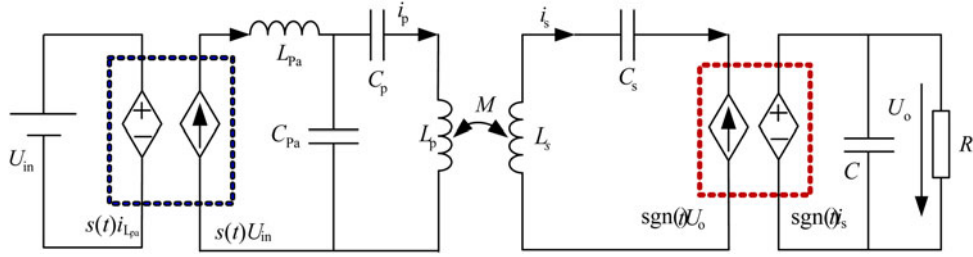


Figure 3. Norton equivalent schematic diagram of the ICPT system.

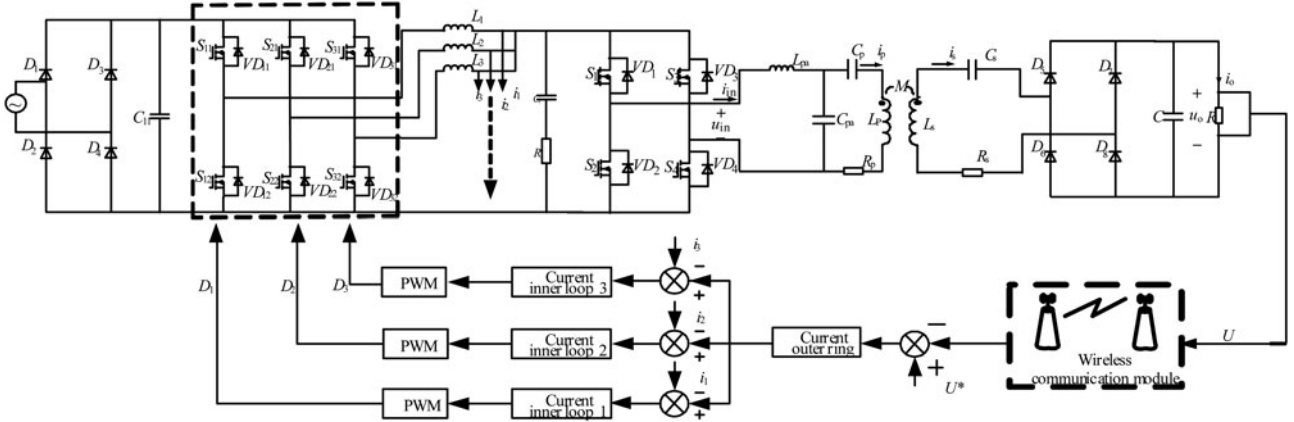


Figure 4. Principle of current sharing and constant voltage output voltage control of the ICPT system.

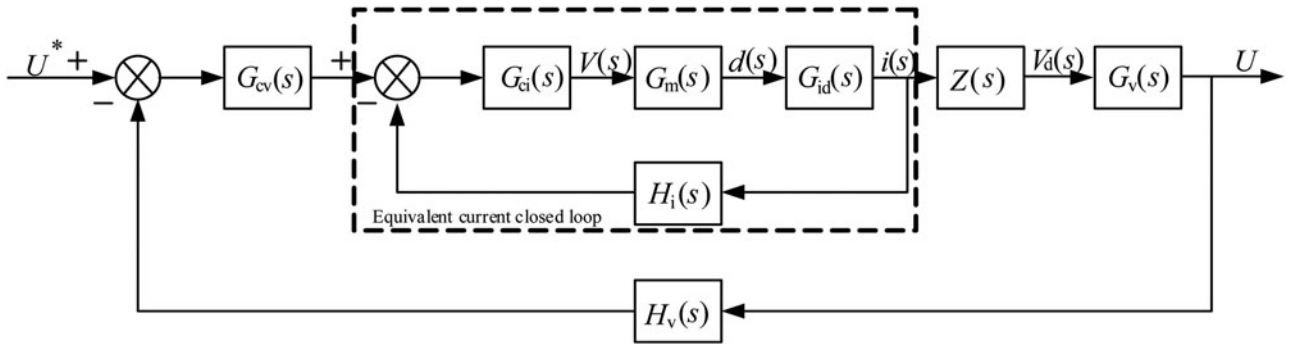


Figure 5. Flow-sharing constant-voltage closed-loop output control block diagram for the ICPT system.

uncompensated current loop can be calculated as:

$$T_i(s) = G_m(s)G_{id}(s)H_i(s) = \frac{6.20 \times 10^{-3}s}{6.08 \times 10^{-10}s^2 + 1.08 \times 10^{-6}s + 1} \quad (6)$$

According to [17], the double-pole double-zero compensation network with an integral is selected. The transfer function of the current loop compensation network is given by equation (7).

$$G_{ci}(s) = \frac{7481(s + 2.025 \times 10^4)^2}{s^2(s + 6.28 \times 10^5)} \quad (7)$$

Then, the frequency characteristic curve of the ICPT system under different conditions is shown in Fig. 6.

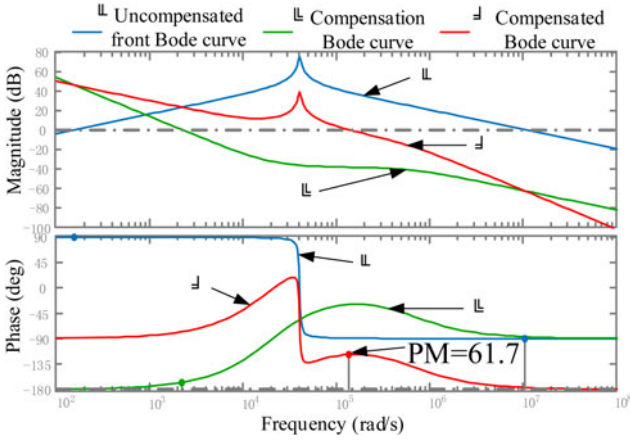
It can be seen from Fig. 6 that the phase margin $PM = 61.7$, which satisfies the demand. The slope of the low-frequency curve is -20 dB/dec and the gain at 0 is large, which can eliminate the steady-state error. The mid-band crosses the 0 dB line with a slope of -20 dB/dec . The slope of the high-frequency band is pulled down and the anti-jamming performance of the system is improved.

Voltage controller design

In order to realize the constant voltage control, the current control loop should be treated as equivalent. From Fig. 5 we can see, the closed-loop transfer function of the current loop and the open-loop gain of the voltage loop with no compensation network are calculated, which can be shown as equations (8) and (9),

Table 1. Parameters of ICPT system

Parameter	Value	Parameter	Value
$C_{11}/\mu\text{F}$	2050	$C_{pa}/\mu\text{F}$	0.0762
$L_1/\mu\text{H}$	77	$C_p/\mu\text{F}$	0.018
$L_2/\mu\text{H}$	77	$L_p/\mu\text{H}$	240
$L_3/\mu\text{H}$	77	$L_s/\mu\text{H}$	240
$C_1/\mu\text{F}$	23.5	$C_s/\mu\text{F}$	0.0146
D	0.75	$C/\mu\text{F}$	68
f_1/kHz	100	R/Ω	27.3
$L_{pa}/\mu\text{H}$	46	k	0.3

**Figure 6.** Current loop frequency characteristic simulation curve.

respectively:

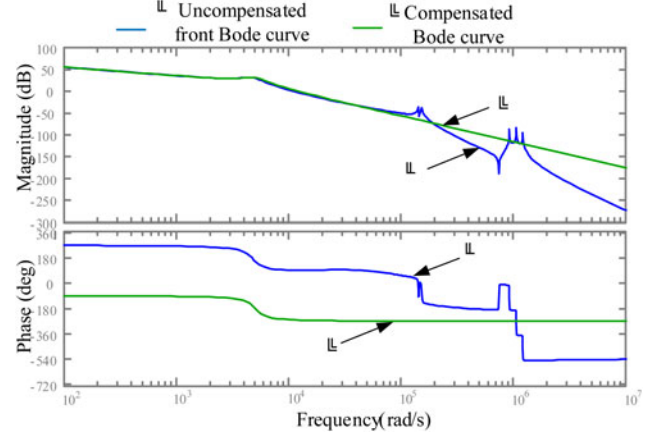
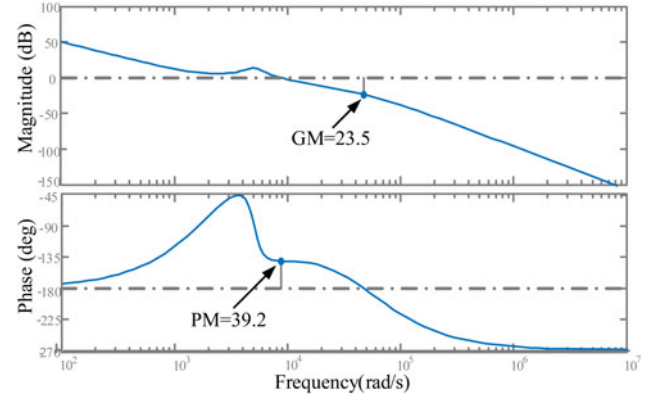
$$B_i(s) = \frac{T_i'(s)}{1 + T_i'(s)}, \quad (8)$$

$$T_v(s) = B_i(s)Z(s)G_v(s)H_v(s). \quad (9)$$

In order to reduce the impact of signal transmission delay on the system, the NRF24L01 module with a transmission rate of 2 Mbps is adopted, which has the characteristics of strong immediacy, ultra-low-power consumption, and high transmission rate. The delay of the module in transmitting 32 bytes of data is <10 ms. Therefore, to make the model more accurate, a delay link is introduced in the voltage feedback transfer function, which is approximated by using an inertia link, that is $H_v(s) = e^{-Ts} \approx 1/(Ts + 1)$, where the delay time is 10 ms.

According to the parameters listed in Table 1, the Bode diagram before and after system fitting is shown in Fig. 7.

It can be found that the open-loop gain function of the voltage loop with no compensation is a high-order function with 19 poles and 12 zero points. In order to simplify the design of the voltage loop controller, the system needs to be reduced by retaining the integral link and a pair of conjugate dominant poles, $-7.83 \times 10^2 - 5 \times 10^3i$, $-7.83 \times 10^2 + 5 \times 10^3i$. The angular frequency corresponding to the dominant pole is 4940 rad/s, so the open-loop

**Figure 7.** Bode diagram before and after system fitting.**Figure 8.** Open-loop gain Bode diagram of the system with the voltage loop compensation network.

gain function after the reduced order is:

$$T_v(s) = \frac{1.6 \times 10^{12}}{s(s^2 + 1566s + 2.561 \times 10^7)}. \quad (10)$$

The green curve in Fig. 7 is the Bode diagram of the system after reduction. It can be found that the reduced-order curve can fit the original curve well.

According to reference [14], the voltage loop design of the converter selects a two-pole three-zero compensation network with an integral, and the final transfer function of the voltage loop compensation network transfer function is:

$$G_{vc}(s) = \frac{9.84(s + 2470)^3}{s(s + 5.34 \times 10^4)^2}. \quad (11)$$

The open-loop gain Bode curve after adding voltage compensation is shown in Fig. 8.

From Fig. 8, it can be seen that the phase margin $PM = 39.2$ and the amplitude-frequency margin $GM = 23.5$, which satisfies the stability index. The mid-band crosses the 0 dB line with a slope of -20 dB/dec and the high-band slope remains at -60 dB/dec and the crossover frequency is 8.74×10^3 rad/s,

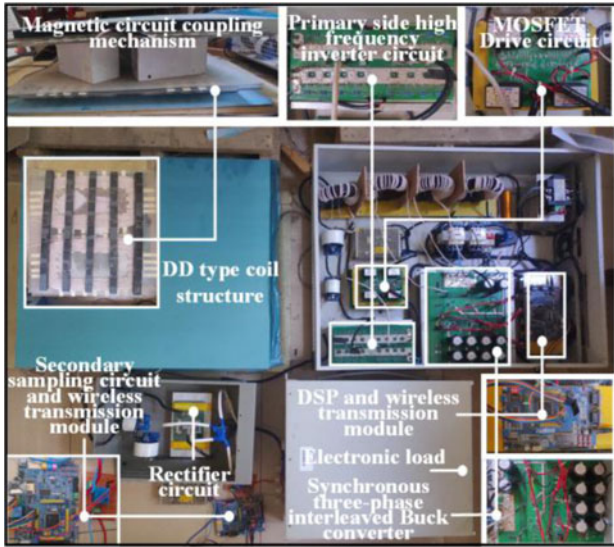


Figure 9. Experimental platform of the ICPT system with current sharing and constant voltage output.

Table 2. Major components

Three-phase Buck circuit	Inverter circuit	Secondary rectifier circuit
Mosfet (six) CREE-C2M0080120D	Mosfet (four) CREE-C2M0080120D	Diode (six) FAIRCHILD-RURG8060

which is close to the design crossover frequency. The indicators meet the design requirements.

Experimental verification

Based on the above theoretical analysis and according to the schematic diagram shown in Fig. 4, the experimental platform shown as in Fig. 9 is built.

The system parameters are shown in Table 1. In this experimental platform, DD coils are used as the primary and secondary coils, the size of them is 4.8 mm in X-direction, and 4.8 mm in Y-direction. In addition, the specifications of the major components in the experimental system are listed in Table 2.

In order to verify the current-sharing and constant-voltage output characteristics of the system under the variation of mutual inductance coupling parameters, the X-direction offset (40 mm) of the DD-type coil is selected in the experiment. For the given offset disturbance, the coupling coefficient decreased from 0.3 to 0.26.

To verify the constant voltage control effect of the controller, the output voltage of the ICPT system U_o and the voltage of the synchronous three-phase triple-parallel Buck converter U_B are measured, which is shown in Fig. 10.

It can be seen from Fig. 10 that the ICPT system can realize 300 V constant voltage output under the coupling coefficient variation. The synchronous three-phase triple-parallel Buck converter can adjust the duty cycle, the output voltage U_B increased from 200 to 226 V, which compensates the drop of output voltage caused by the coupling coefficient variation. The experimental results have verified the effectiveness of the controller design.

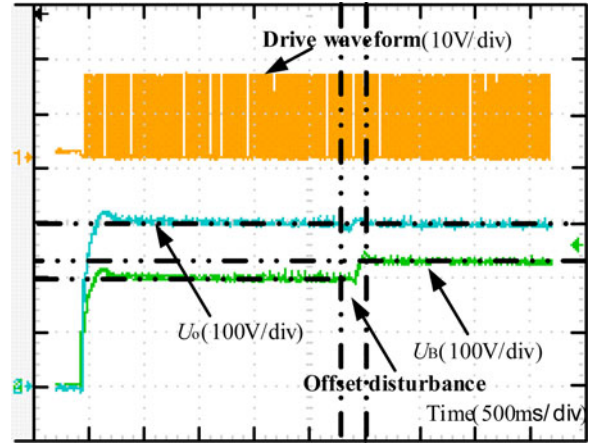


Figure 10. Drive and output voltage waveforms of the output voltage and the synchronous three-phase triple-parallel Buck converter.

To verify the current sharing effect of the controller, the three-phase inductor current ripple of the synchronous three-phase triple-parallel Buck converter is shown in Fig. 11.

It can be seen from Fig. 11 that, before and after coupling coefficient variation, the three-phase inductor currents of the synchronous three-phase parallel Buck converter are almost the same, which verified the effectiveness of the current sharing controller.

In order to verify the effectiveness of the circuit parameter design and calculate the efficiency of the system, the output voltage of the inverter and the primary side coil current waveform before and after the coupling coefficient variation are shown in Fig. 12. The secondary side pickup voltage and the waveforms are collected as in Fig. 13.

It can be seen from Figs 12 and 13 that before and after the coupling coefficient variation, the inverter output voltage U_{in} always leads the primary side transmitting coil current I_p 90°, and the secondary side pickup voltage U_s is always in phase with the secondary side current I_s , which satisfies the LCC-S compensation network topology, and proves the correctness of the system parameter design.

It can be seen from Fig. 12, the amplitude of the square wave of the inverter rises to 226 V, and the effective value of the primary current rises to about 9 A, which compensates for the voltage drop caused by the decrease of the coupling coefficient and achieves 3.3 kW power transfer with a constant voltage.

It can be seen from Fig. 13 that the pickup voltage and current are always constant before and after the coupling coefficient variation. The pickup voltage amplitude is 300 V, and the secondary current amplitude is always about 17.3 A. At the same time, according to the experimental result, the effective value of the primary input current, that is the primary rectifier circuit, reaches 17.5 A. After calculation, the overall efficiency of the system is about 86%.

In order to further verify the effectiveness of the current sharing constant voltage controller under the load variation, the experiment from 3.3 kW full load (load resistance 27.3 Ω) to 1.67 kW half load (load resistance 54 Ω) is done. The output voltage waveform and the three-phase inductor current waveforms of the system are shown in Figs 14 and 15.

It can be seen from Fig. 14 that before and after the load variation, the system output maintains a constant value, which is 300

Figure 11. Output voltage and inductor current waveforms of the synchronous three-phase triple-parallel Buck converter before and after coupling coefficient variation. (a) Before coupling coefficient variation. (b) After coupling coefficient variation.

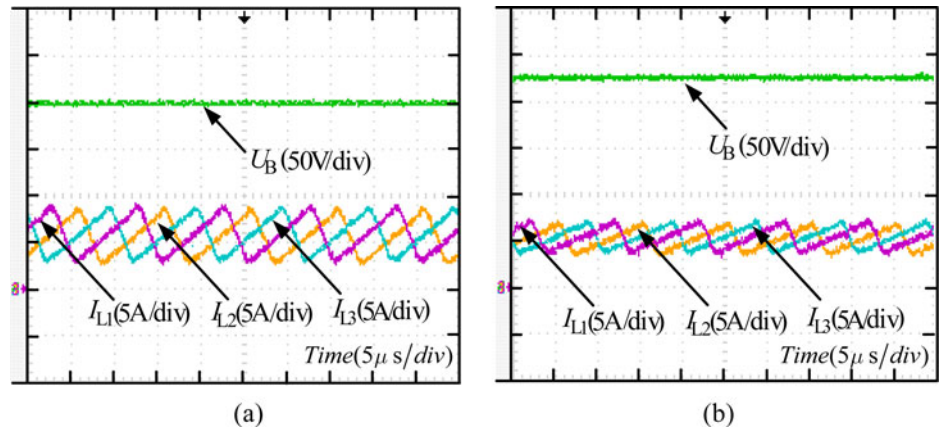


Figure 12. Output voltage and primary side coil current waveform of the inverter before and after coupling coefficient variation. (a) Before coupling coefficient variation. (b) After coupling coefficient variation.

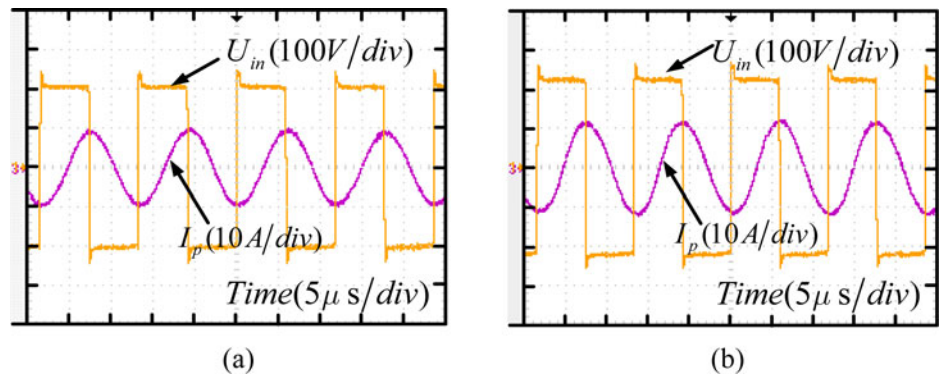


Figure 13. Voltage and current waveform of the secondary side pick-up before and after coupling coefficient variation. (a) Before coupling coefficient variation. (b) After coupling coefficient variation.

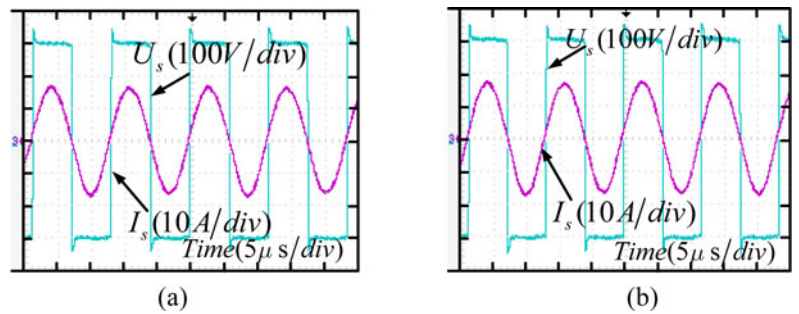


Figure 14. Drive and output voltage waveforms of the system output voltage and the synchronous three-phase triple-parallel Buck converter.

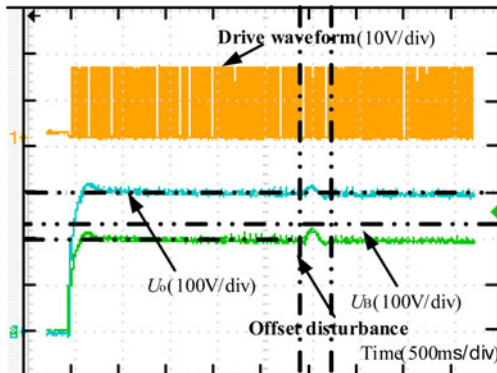


Figure 15. Output voltage and inductance current waveforms of the synchronous three-phase triple-parallel Buck converter under full and half load conditions. (a) Full load. (b) Half load.

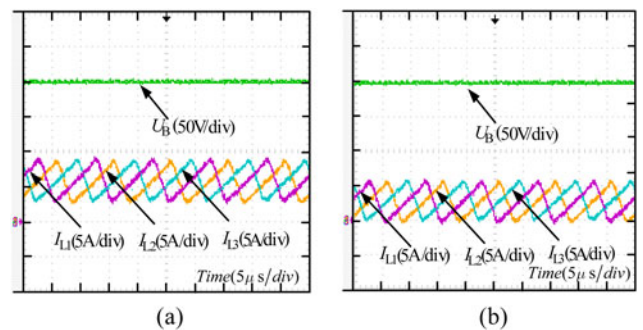


Table 3. Comparison of sign-phase Buck converter and three-phase triple-parallel Buck converter

	Fault tolerance	Switch tube stress	Voltage ripple	Power density	Redundancy	Volume	Cost
Single-phase Buck converter	No	Larger	Larger	Larger	Lower	A	S
Three-phase triple-parallel Buck converter	Yes	Smaller	Smaller	Smaller	Higher	<3A	<3S

V, and the synchronous three-phase triple-parallel Buck converter keeps a constant voltage output of 200 V.

It can be seen from Fig. 15 that when the ICPT system works from 3.3 kW full load mode to half load mode, the average value of the inductor of each phase of the synchronous three-phase triple-parallel Buck converter drops from 5.67 to 2.9 A. It can be seen that the three-phase inductor currents of the synchronous three-phase triple-parallel Buck converter are always balanced with load variation, which verifies the effectiveness of the constant voltage and current sharing control under load variation.

Besides, the cost and performance by comparing a single-phase Buck converter with a three-phase triple-parallel Buck converter are shown as Table 3.

Where A represents the volume of a single-phase Buck converter, and S represents the cost of a single-phase Buck converter. It can be seen that although more devices are used in the synchronous triple-parallel Buck converter, the cost and volume are larger, the performance is much better, so it is widely used in high-power ICPT system.

Conclusion

In this paper, a 3.3 kW ICPT system with a synchronous three-phase triple-parallel Buck converter is built. In this system, aimed at the influence of the coupling coefficient variation, the GSSA model is used to model the LCC-S resonant converter, and the small-signal model is used to model the three-phase triple-parallel Buck converter. In addition, based on the frequency-domain method, the methods of the three-phase current sharing of the synchronous three-phase triple-parallel Buck converter and the constant voltage output control of the ICPT system under coupling coefficient variation are studied. The theoretical and experimental results show that the current sharing and the constant voltage output are better under the coefficient variation and demonstrate the stability of the ICPT system.

Acknowledgement. This work is supported by the State Grid Corporation of China Headquarter Science and Technology Project (Research on Series Design of Electric Vehicle Wireless Charging System and Equipment Development).

References

- Xia C, Zhu W, Ma N, Jia R and Yu Q (2018) A load identification method for ICPT system utilizing harmonics. *Journal of Electrical Engineering & Technology* **13**, 2178–2186.
- Li Y, Sun Y and Dai X (2013) μ -Synthesis for frequency uncertainty of the ICPT system. *IEEE Transactions on Industrial Electronics* **60**, 291–300.
- Madawala UK and Thrimawithana DJ (2011) A bidirectional inductive power interface for electric vehicles in V2G systems. *IEEE Transactions on Industrial Electronics* **58**, 4789–4796.
- Badr BM, Somogyi-Csizmazia R, Leslie P and Delaney KR (2017) Design of a wireless measurement system for use in wireless power transfer applications for implants. *Wireless Power Transfer* **4**, 21–32.
- Zhang Z, Zhang B, Deng B, Wei X and Wang J (2018) Opportunities and challenges of metamaterial-based wireless power transfer for electric vehicles. *Wireless Power Transfer* **5**, 9–19.
- Xia C, Xie G, Lin K, Chen G, Ren and Zhang Y (2016) Study of dual resonance point characteristics and maximum output power of ICPT based on double LCL compensation. *Proceedings of the CSEE* **36**, 5200–5209.
- Xia C, Wang W, Chen G, Wu X, Zhou S and Sun Y (2017) Robust control for the relay ICPT system under external disturbance and parametric uncertainty. *IEEE Transactions on Control Systems Technology* **25**, 2168–2175.
- Li Y, Du H, Yang M and He Z (2018) Two-Degree-of-Freedom h infinity robust control optimization for the IPT system with parameter perturbations. *IEEE Transactions on Power Electronics* **33**, 10954–10969.
- Van DPFFA, Castilla M and Bauer P (2013) Adaptive Sliding-Mode control for a Multiple-User inductive power transfer system without need for communication. *IEEE Transactions on Industrial Electronics* **60**, 271–279.
- Narimani M and Moschopoulos G (2014) An investigation on the novel use of High-Power Three-Level converter topologies to improve Light-Load efficiency in low power DC/DC Full-Bridge converters. *IEEE Transactions on Industrial Electronics* **61**, 5690–5692.
- Luo B, Chen L and Li Y (2017) Investigation of output voltage control for the inductive power. *Transactions of China Electrotechnical Society* **32**, 235–242.
- Zhang X, Xu J, Bao B and Zhou G (2016) Asynchronous-Switching Map-Based stability effects of circuit parameters in fixed Off-Time controlled buck converter. *IEEE Transactions on Power Electronics* **31**, 6686–6697.
- Hu A P and Hussmann S (2004) Improved power flow control for contactless moving sensor applications. *IEEE Power Electronics Letters* **2**, 135–138.
- Wang J, Tzeng L, Hsu M and Jian H (2018) A simple control scheme to avoid the sensing noise for the DC-DC buck converter with synchronous rectifier. *IEEE Transactions on Industrial Electronics* **65**, 5086–5091.
- Orabi M and Shawky A (2015) Proposed switching losses model for integrated Point-of-Load synchronous buck converters. *IEEE Transactions on Power Electronics* **30**, 5136–5150.
- Hu A P (2009) Modeling a contactless power supply using GSSA method. *Proc. IEEE Int. Conf. Ind. Technol.*, 1–6.
- Maksimovic D and Zane R (2007) Small-signal discrete-time modeling of digitally controlled PWM converters. *IEEE Transactions on Power Electronics* **22**, 2552–2556.
- Huang X, Peng Y and Li Y (2013) Current balancing for three-phase buck-type interleaving parallel rectifier. *Power Electronics* **47**, 81–83.



Songcen Wang was born in Henan Province, China, in 1979. He received his B.S degree in Control Theory and Control Engineering from North China Electric Power University, Beijing, China, in 2001, and the M.S. and Ph.D. degrees in Power Electronics from China Electric Power Research Institute (CEPRI), in 2004 and 2010, respectively. From November 2014 to October 2015, he was an academic visitor at the Aalborg University, Denmark. He is presently working as a Senior Engineer in the Department of Electrical Engineering in CEPRI. His current research interests include wireless power transfer and power electronics.



Xiaokang Wu was born in Beijing, China, in 1991. He received his M.S. degree in Tianjin Polytechnic University, Tianjin, China. He is currently an engineer in China Electric Power Research Institute (CEPRI), Beijing, China. His current research interest includes Wireless Power Transmission technology.



Zhen Wu was born in Jiangsu Province, China, in 1995. He received his B.S. degree in the School of Electrical and Power Electrical from China University of Mining and Technology, Xuzhou, China, in 2018. He is currently working toward his M.S. degree in the School of Electrical and Power Engineering, China University of Mining and Technology, Xuzhou, China. His current research interests include wireless

power transfer and its application.



Ying Yang was born in Jiangsu Province, China, in 1994. She received her B.S. degree in Electrical Engineering and Automation from the Nanjing University of Information Science and Technology, Jiangsu, China, in 2017. She is currently working toward her M.S. degree in the School of Electrical and Power Engineering, China University of Mining and Technology, Xuzhou, China. Her current

research interests include wireless power transfer and its application.



Chenyang Xia was born in Jiangsu Province, China, in 1982. He received his B.S., M.S., and Ph.D. degrees in Control Theory and Control Engineering from Chongqing University, Chongqing, China, in 2006, 2008, and 2010, respectively. From August 2018 to August 2019, he was an Academic Visitor at the University of Auckland, Auckland, New Zealand. He is presently working as an

Associate Professor in the School of Electrical and Power Engineering, China University of Mining and Technology, Xuzhou, China. His current research interests include wireless power transfer and intelligent control.



Cong Zhu He was born in JiangSu Province, China, in 1993. He received the B.S. degree in Electrical Engineering and Automation from Jiangsu Normal University, Xuzhou, China, in 2016. He is currently working toward his M.S. degree in the School of Electrical and Power Engineering, China University of Mining and Technology. His current research interests include wireless power transfer.